PHYSICAL REVIEW B **72**, 144427 (2005)

Magnetic properties of selected Mn-based transition metal compounds with β-Mn structure: Experiments and theory

T. Eriksson,[1] L. Bergqvist,[2] Y. Andersson,[1] P. Nordblad,[3] and O. Eriksson[2]
[1]*Department of Materials Chemistry, Uppsala University, Box 538, SE-751 21 Uppsala, Sweden*
[2]*Department of Physics, Uppsala University, Box 530, SE-751 21 Uppsala, Sweden*
[3]*Department of Engineering Sciences, Uppsala University, Box 534, SE-751 21 Uppsala, Sweden*

(Received 11 March 2005; revised manuscript received 27 June 2005; published 28 October 2005)

Two compounds, Mn_3CoSi and Mn_3CoGe have been synthesized and found to crystallize in the $AlAu_4$ type structure, an ordered form of the β-Mn structure. The magnetic structure and properties have been studied by magnetometry and neutron powder diffraction and the theoretical work is based on first principles total energy calculations. Comparison is made with the magnetic properties of the isostructural compounds Mn_3IrGe and Mn_3IrSi. The solid solutions $Mn_3Ir_{1-y}Co_ySi$ $(0 \leqslant y \leqslant 1)$ and $Mn_3CoSi_{1-x}Ge_x$ $(0 \leqslant x \leqslant 1)$ are also studied. A noncollinear antiferromagnetic structure is experimentally observed for $y=0.20$ as well as for $x=0.50$ and 1.0, similar to that of Mn_3IrSi and Mn_3IrGe, with 120° angles between magnetic moments on a triangular network of Mn atoms, and this finding is corroborated by theoretical calculations. For $y=0.80$–1.0 a transformation to a new type of magnetic structure takes place. The magnetic transition temperature decreases on decreasing unit cell dimension, with good qualitative agreement with the decay of the calculated interatomic exchange energy. Both theory and experiments find the magnitude of the Mn magnetic moment to decrease on decreasing unit cell volume, the same trend is found in calculations for β-Mn.

DOI: 10.1103/PhysRevB.72.144427 PACS number(s): 75.25.+z, 61.66.−f, 71.20.−b, 75.30.Cr

I. INTRODUCTION

We have recently reported interesting magnetic properties of Mn_3IrSi and Mn_3IrGe.[1,2] Both compounds form commensurate noncollinear antiferromagnetic structures. The near neighbor Mn magnetic moments are found on three-dimensional networks of corner linked triangles, resulting in geometrically frustrated antiferromagnetic interactions that lead to 120° angles between the projections of the magnetic moments on the triangle planes.[1,2] The magnetic structures of Mn_3IrSi and Mn_3IrGe are particularly interesting in view of the close structural relationship with β-Mn, a polymorph of manganese that does not order magnetically.[3] The Mn atoms in Mn_3IrSi and Mn_3IrGe are situated in a 12-fold site similar to the *12d* site of β-Mn, whereas the Ir and Si/Ge atoms occupy two different fourfold sites derived by splitting the *8c* site of β-Mn. It is not fully understood why replacing some of the Mn atoms in β-Mn with elements that show no magnetic ordering, such as Ir, Si, and Ge, gives rise to magnetic order.

Numerous experimental studies have been devoted to the lack of a long-range magnetically ordered state in β-Mn, including investigations of alloys of β-Mn with, for example, Al,[4–6] Sn,[7,8] Co,[9,10] Ru,[11] and Ir.[12] The β-Mn(Al) system shows strong spin fluctuations with antiferromagnetic Mn-Mn interactions that at low temperatures are slowed down for alloyed samples, suggesting that β-Mn is in a spin liquid state and forms a low temperature spin-glass state on alloying.[4,5] The dominating magnetic interactions are found to take place between Mn atoms in the 12-fold site ($\sim$1 μ_B/atom) whereas negligible magnetic moments are found for the Mn atoms in the eightfold site. The lack of long range magnetic order in β-Mn was therefore suggested to be an effect of geometric frustration of magnetic moments on the three-dimensional triangular network formed by the 12-fold site Mn atoms. This view was recently challenged by Hafner and Hobbs,[13] who by first principles spin-density functional calculations found a ferrimagnetic ground state at slightly expanded volumes, with volume dependent magnetic moments on both the *8c* and *12d* Mn atoms (up to 3–4 μ_B/atom at strongly expanded volume), and thus they concluded that the antiferromagnetic couplings are strongest between the *8c* and *12d* Mn atoms. Together the Mn atoms in the *12d* and *8c* sites form a network of tetrahedra—another source of geometric frustration.

This paper attempts to investigate if, similar to Mn_3IrSi and Mn_3IrGe, the isoelectronic compounds Mn_3CoSi and Mn_3CoGe can be synthesized, and if the same noncollinear long range magnetic order is stable for these compounds, despite the fact that for some of them the volume is expected to be lower than that of β-Mn. In a broader context we aim to identify the mechanisms that govern the magnetic properties, not only of Mn_3CoSi and Mn_3CoGe and their alloys with Ir, but also of the lively debated β-phase of Mn.

The ternary phase diagram of Mn-Co-Si at 800 °C was studied by Kuz'ma[14,15] and the metal rich section at 1000 °C by Bardos *et al.*,[16] but the existence of an ordered Mn_3CoSi phase was not reported. At 1000 °C the Mn_3CoSi composition is at the border of the extended β-Mn phase field, whereas at 800 °C it is in a two phase region of β-Mn+ "S-phase." For Mn-Co-Ge only the Mn rich corner of the ternary phase diagram at 1000 °C was established, without reports of an ordered Mn_3CoGe phase, and with the β-Mn phase field extending only to $\sim$7 at. % Si for 20 at. % Co.[16]

This paper describes the preparation and characterization of the new phases Mn_3CoGe and Mn_3CoSi, as well as the solid solutions $Mn_3Ir_{1-y}Co_ySi$ and $Mn_3CoSi_{1-x}Ge_x$. The crystal and magnetic structures were determined by neutron powder diffraction and the magnetic properties were studied by SQUID magnetometry. The theoretical work was based on first principles theory using a noncollinear version[17] of the linear muffin-tin orbital method (LMTO) in the atomic sphere approximation (ASA) and a Korringa-Kohn-Rostoker method in the atomic sphere approximation (KKR-ASA).

II. EXPERIMENT

A. Sample preparation and phase analysis

Samples of compositions Mn_3CoSi, Mn_3CoGe, $Mn_3CoSi_{0.50}Ge_{0.50}$, $Mn_3Ir_{0.20}Co_{0.80}Si$, and $Mn_3Ir_{0.80}Co_{0.20}Si$ were prepared from appropriate amounts of the elements, by the drop-synthesis method.[18] A high frequency vacuum induction furnace with 300 mbar argon atmosphere was used, with the samples contained in alumina crucibles. Starting materials were single crystal pieces of silicon (Highways International, purity 99.999%), and/or germanium (Highways International, purity 6 N), pressed pellets of iridium powder (Cerac, purity 99.9%), cobalt metal rod (Johnson and Matthey, spec. pure) and pieces of manganese metal (Cerac, claimed purity 99.99%, purified from manganese oxides by sublimation). Compounds of $Mn_3Ir_{1-y}Co_ySi$ with $y=0.40$, 0.60 and of $Mn_3CoSi_{1-x}Ge_x$ with $x=0.975$, 0.950 were prepared by melting appropriate amounts of the above samples in an arc furnace under 300 mbar argon atmosphere. All samples were annealed in evacuated fused silica tubes at 900 °C for 4–8 days and 800 °C for 1–3 weeks and subsequently quenched in water. The samples investigated by neutron diffraction techniques were stress-relieved at 800 °C for 25–30 minutes.

Phase analysis and determination of unit cell parameters were performed by recording x-ray powder diffraction films with a Guinier-Hägg focusing camera, using Cu $K\alpha_1$ radiation. Silicon or germanium powders were added as internal standard for calibration ($a=5.4309$ Å and $a=5.6576$ Å, respectively, at 25 °C).

B. Neutron powder diffraction

Neutron powder diffraction data were collected at the R2 research reactor at NFL in Studsvik, Sweden, for $Mn_3CoSi_{1-x}Ge_x$ ($x=1.0$, 0.50) at temperatures 295, 90, 10 K, and for $Mn_3Ir_{1-y}Co_ySi$ at 295, 120, 75, 10 K ($y=1.0$), and at 295 and 10 K ($y=0.20$, 0.80), respectively. The measurements were performed in the 2θ-range 4–140° in steps of 0.08°, with the samples contained in vanadium cylinders. A parallel double Cu (220) monochromator system was used, giving the wavelength 1.471 Å. An absorption correction was applied using $\mu R=0.232$, 0.259 for $x=1.0$, 0.50, and $\mu R=0.251$, 0.282, 0.655 for $y=1.0$, 0.80, 0.20, respectively, as calculated from transmission measurements at $2\theta=0°$.

Structure refinements were performed by the Rietveld method, using the program FULLPROF[19] with the scattering lengths Mn, −3.73 fm; Ir, 10.60 fm; Co, 2.49 fm; Si, 4.149 fm; Ge, 8.185 fm. The pseudo-Voigt function was used to describe the peak shape and the background was modeled by interpolation between fixed points. For the 295 K data sets, 16 parameters were varied. Profile parameters: 2θ zero point (1), scale factor (1), profile shape parameter (1), half-width parameters (3), asymmetry parameters (2). Structural parameters: atomic coordinates (5), lattice parameter (1), isotropic temperature factors (2). For the 10 K data sets of the $x=1.0$, 0.50 and $y=0.20$ samples and the 90 K data sets of the $x=1.0$, 0.50 samples, the x,y and z components of a magnetic moment localized on the manganese atoms were varied, as well as the profile and structural parameters listed above, with the exception that an overall isotropic temperature factor was used (17 varied parameters). The nuclear and magnetic contributions to the diffraction intensities were treated as two separate phases, with the magnetic phase described in space group $P\bar{1}$, using the magnetic form factor coefficient of Mn(0).[20]

C. Magnetization measurements

A Quantum Design MPMSXL SQUID magnetometer was used to measure the macroscopic magnetic response of the samples. Magnetization vs temperature scans in a field of 250 Oe were performed in zero field cooled (zfc) and field cooled (fc) procedures in the temperature range 10 to 300 K (zfc) and back to 10 K (fc). Measurements of magnetization vs field were made at some different temperatures. In addition, one of the samples, that showed indications of spin glass behavior, was investigated by ac susceptibility at different frequencies at temperatures close to the observed transition temperature.

III. THEORY

The electronic structure and total energy calculations were all based on density functional theory (DFT) in the local spin density approximation. Two different methods have been applied in the calculations, namely a noncollinear linear-muffin-tin orbital (LMTO) method[17] and the Korringa-Kohn-Rostoker Green's function method in the atomic sphere approximation (KKR-ASA).[21,22] Both methods are able to handle noncollinear spins where the magnetic moment can point in any general direction in space and not only up or down. The calculations are converged both in number of k points inside the Brillouin zone and the number of basis functions (s,p,d for all atomic species), e.g., the LMTO calculations employed 216 k points in the Brillouin zone and the KKR-ASA calculations used 245 k points. The Brillouin zone integration employed the method of Methfessel and Paxton[23] for the LMTO and KKR calculations. Further, the local density approximation was used with the parametrization of Perdew, Burke, and Ernzerhof.[24] The exchange parameter J_0, which is the sum of all pair exchange interactions J_{ij} in an effective Heisenberg model,[25] was calculated from the site-diagonal blocks of the Green's function in the KKR method.

IV. RESULTS

A. Phase analysis

X-ray powder diffraction films recorded for the substitution series $Mn_3Ir_{1-y}Co_ySi$ ($0\leqslant y\leqslant 1$) show all samples to be

TABLE I. Lattice parameter of $Mn_3Ir_{1-y}Co_ySi_{1-x}Ge_x$ at 295 K.

Composition	Lattice parameter (Å)
Mn_3IrSi	6.4973(3)[a]
$Mn_3Ir_{0.80}Co_{0.20}Si$	6.4542(2)
$Mn_3Ir_{0.60}Co_{0.40}Si$	6.4107(3)
$Mn_3Ir_{0.40}Co_{0.60}Si$	6.3592(2)
$Mn_3Ir_{0.20}Co_{0.80}Si$	6.2992(2)
Mn_3CoSi	6.2446(2)
$Mn_3CoSi_{0.50}Ge_{0.50}$	6.3219(2)
$Mn_3CoSi_{0.050}Ge_{0.950}$	6.3895(2)
$Mn_3CoSi_{0.025}Ge_{0.975}$	6.3929(2)
Mn_3CoGe	6.3953(1)

[a] From Ref. 1.

phase pure. A complete range of solid solubility occurs between Mn_3IrSi and Mn_3CoSi, with a close to linear concentration dependence of the primitive cubic unit cell parameter, see Table I. A systematic concentration dependence of the unit cell parameter is also observed for the substitution series $Mn_3CoSi_{1-x}Ge_x$ $(0 \leqslant x \leqslant 1)$, Table I. For samples with $x=0.0$, 0.50 all observed reflections are indexed by the primitive cubic unit cell of $Mn_3CoSi_{1-x}Ge_x$, whereas for $x=1.0$, 0.975, 0.950 a few very weak reflections that could not be indexed by this cubic unit cell were observed, the strongest was found for Mn_3CoGe $(x=1.0)$.

B. Crystal structure

The $AlAu_4$ type structure,[26] an ordered form of the β-Mn type structure,[27] is adopted at all studied compositions, as evidenced, e.g., by the (200) reflection in the 295 K neutron powder diffraction patterns (symmetry forbidden for the β-Mn type structure). With the space group symmetry $P2_13$, two inequivalent $4a$ sites are occupied by silicon-germanium and iridium-cobalt, respectively, and the $12b$ site is occupied by manganese. Thus Mn_3CoSi and Mn_3CoGe are isostructural with the recently reported compounds Mn_3IrGe and Mn_3IrSi.[1,2] The unit cell contains four formula units. Table II lists the structural parameters obtained from refinements by the Rietveld method, for neutron diffraction data collected at 295 K for all studied compositions. The observed and calculated neutron diffraction profiles are shown in Fig. 1 for Mn_3CoGe and in Fig. 2 for Mn_3CoSi.

Weak extra reflections can be observed in the Mn_3CoGe diffraction profile and the corresponding regions were excluded from the structure refinements. The presence of minor amounts of additional phases suggests that a small deviation from the ideal composition may occur for the Mn_3CoGe phase. Attempts at refining the occupancies (keeping the temperature factors fixed), resulted in a small substitution of Mn on the Co site (~4% Mn, corresponding to about five standard deviations), with small improvements of the agreement factors ($R_{wp}=5.03\%$, $R_{Bragg}=5.97\%$, compared to $R_{wp}=5.08\%$, $R_{Bragg}=6.21\%$ for the Mn_3CoGe composition). Also for $Mn_3CoSi_{0.50}Ge_{0.50}$, minor amounts of Mn (~2%, corresponding to about 3.5 standard deviations) are obtained on the Co site, when varied, with small improvements of the agreement factors ($R_{wp}=3.86\%$, $R_{Bragg}=4.72\%$, compared to $R_{wp}=3.88\%$, $R_{Bragg}=4.90\%$ for the $Mn_3CoSi_{0.50}Ge_{0.50}$ composition), whereas the Si and Ge occupancies did not vary significantly from $x=0.50$. For Mn_3CoSi no significant deviation from full site occupancy was found. The refined occupancies were not significantly different from the compositions $Mn_3Ir_{0.20}Co_{0.80}Si$, and $Mn_3Ir_{0.80}Co_{0.20}Si$, respectively, for the substituted samples.

Interatomic distances up to 3.2 Å at 295 K were calculated and are listed in Table III. The closest Mn-Mn distances are found on a network of equilateral triangles, with each corner (Mn atom) shared between three triangles with slightly different side lengths, as illustrated in a drawing of the unit cell in Fig. 3. As may be expected the interatomic distances increase with increased unit cell volume, with the notable exception of $Mn_3Ir_{0.20}Co_{0.80}Si$, for which the shortest and longest listed Mn-Mn distances are markedly shorter and longer, respectively, than expected. The deviation is due to somewhat different Mn coordinates for this composition.

C. Magnetic properties

The most prominent feature of all samples is that the susceptibility (M/H) varies weakly with temperature, and is of similar magnitude $(10\text{–}20 \times 10^{-6}$ emu/g G) for all compositions. A small maximum in the zfc susceptibility curves indicates that magnetic ordering without a dominating macroscopic spontaneous magnetic moment occurs in the samples. In addition, all samples show a closely linear response vs magnetic field both above and below the maximum in the susceptibility.

In Figs. 4 and 5, the zfc and fc susceptibility curves of the samples in the series $Mn_3Ir_{1-y}Co_ySi$ and the two samples $Mn_3CoSi_{0.50}Ge_{0.50}$ and Mn_3CoGe are shown, respectively. The transition temperatures were derived from the maximum of the $d(\chi_{zfc}T)/dT$ curves for all samples in the series. Substituting Ir for Co initially causes a continuous decrease of the transition temperature from 210 K (Mn_3IrSi) to 70 K ($Mn_3Ir_{0.20}Co_{0.80}Si$), however with a changed trend back to 100 K for Mn_3CoSi. Substitution of Si for Ge gives higher transition temperatures, 125 K for $Mn_3CoSi_{0.50}Ge_{0.50}$ and 145 K for Mn_3CoGe. Most of the samples show some irreversibility between the zfc and fc susceptibility below the transition temperature, which implies that the antiferromagnetic compensation of the moments is imperfect. The clearest appearance of irreversibility just at T_N and the largest difference between the zfc and the fc M/H curves is seen for Mn_3CoGe, where one from Fig. 5 measures a difference of 0.01 emu/g at 10 K. This could correspond to a spin configuration where 1 out of 10 000 Mn moments is uncompensated.

The curves of magnetization vs field are closely linear for all samples both above and below the transition temperatures. In the low temperature region, the slope of these curves is governed by the zfc M/H magnitude, implying that the difference between zfc and fc curves at temperatures below T_N emanates from spontaneous uncompensated spins

TABLE II. Structural parameters for $Mn_3Ir_{1-y}Co_ySi_{1-x}Ge_x$ at 295 K. Estimated standard deviations within parentheses. Space group $P2_13$.

Atom	Wyckoff pos.	x	y	z	B_{iso}(Å^2)
Mn_3CoSi					
Mn	12*b*	0.1319(8)	0.2029(8)	0.4520(8)	0.58(2)
Co	4*a*	0.686(1)	0.686	0.686	0.67(4)
Si	4*a*	0.0641(9)	0.0641	0.0641	0.67[a]
R_p=3.39%; R_{wp}=4.24%; R_{exp}=3.39%; χ^2=1.56; R_{Bragg}=4.57%					
Mn_3CoGe					
Mn	12*b*	0.1267(7)	0.2021(6)	0.4540(7)	0.76(4)
Co	4*a*	0.685(1)	0.685	0.685	0.51(3)
Ge	4*a*	0.0630(3)	0.0630	0.0630	0.51[a]
R_p=3.91%; R_{wp}=5.08%; R_{exp}=3.72%; χ^2=1.86; R_{Bragg}=6.21%					
$Mn_3CoSi_{0.50}Ge_{0.50}$					
Mn	12*b*	0.1286(6)	0.2009(5)	0.4539(6)	0.58(3)
Co	4*a*	0.6864(9)	0.6864	0.6864	0.47(2)
Si/Ge	4*a*	0.0650(4)	0.0650	0.0650	0.47[a]
R_p=3.07%; R_{wp}=3.88%; R_{exp}=3.16%; χ^2=1.51; R_{Bragg}=4.90%					
$Mn_3Ir_{0.80}Co_{0.20}Si$					
Mn	12*b*	0.123(1)	0.207(1)	0.4541(8)	0.90(5)
Ir/Co	4*a*	0.6839(4)	0.6839	0.6839	0.45(2)
Si	4*a*	0.0659(9)	0.0659	0.0659	0.45[a]
R_p=3.58%; R_{wp}=4.57%; R_{exp}=4.03%; χ^2=1.28; R_{Bragg}=4.47%					
$Mn_3Ir_{0.20}Co_{0.80}Si$					
Mn	12*b*	0.1391(8)	0.2087(6)	0.4494(6)	0.63(3)
Ir/Co	4*a*	0.684(1)	0.684	0.684	0.72(2)
Si	4*a*	0.065(1)	0.065	0.065	0.72[a]
R_p=3.13%; R_{wp}=3.95%; R_{exp}=3.57%; χ^2=1.28; R_{Bragg}=4.89%					

[a] The isotropic temperature factors of Ir/Co and Si/Ge were constrained to have the same value.

that get locked along the fc field at low temperatures. The appearance of irreversibility between low field zfc and fc susceptibility curves for antiferromagnetic samples is quite common, in fact, both for some pure[28] and always for diluted antiferromagnets.[29]

An alternative explanation for the observed irreversible behavior of the zfc and fc susceptibility could be a spin-glass transition; especially the $Mn_3Ir_{0.20}Co_{0.80}Si$ sample shows a behavior that resembles that of a spin glass. However, measurements of low field (3 Oe) ac-susceptibility at different frequencies (1.7, 17, and 170 Hz) did not reveal a clear spin-glass characteristic frequency dependence of the maximum, or the appearance of an out of phase component of the susceptibility.

D. Experimental magnetic structure

The magnetic contributions in the neutron powder diffraction patterns recorded at 10 K for Mn_3CoGe, $Mn_3CoSi_{0.50}Ge_{0.50}$, and $Mn_3Ir_{0.80}Co_{0.20}Si$ are superimposed on some of the Bragg reflections from the crystal structure, similar to the previously published neutron powder diffrac-

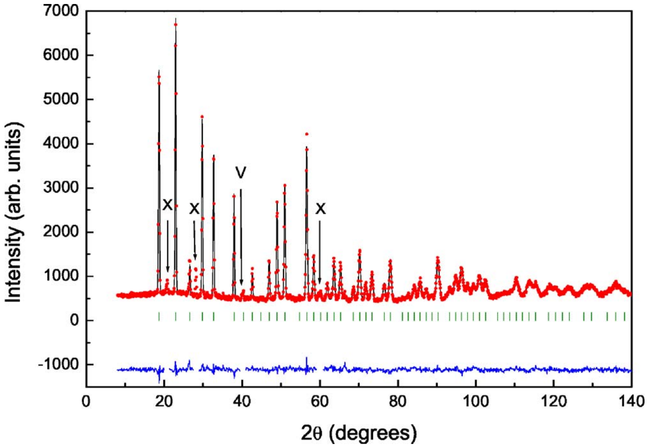

FIG. 1. (Color online) Observed (points), calculated (solid line) and difference (bottom solid line) neutron powder diffraction profiles for Mn_3CoGe at 295 K. Tick marks indicate the positions of Bragg reflections. The regions excluded from the refinement correspond to peaks from impurity phases (marked with "X"), and a minor peak from the vanadium sample holder, partly overlapping a peak from the crystal structure (marked with "V").

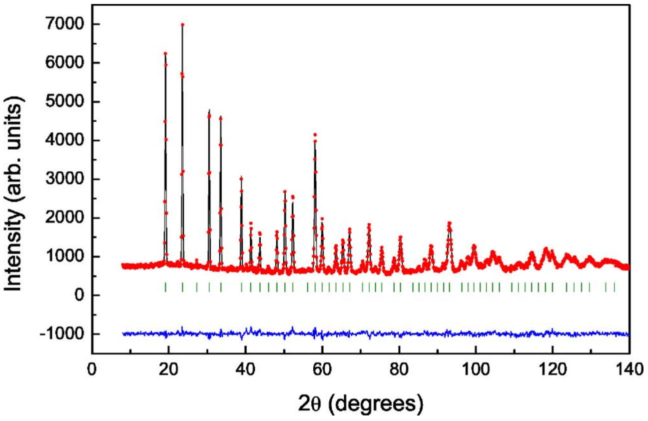

FIG. 2. (Color online) Observed (points), calculated (solid line) and difference (bottom solid line) neutron powder diffraction profiles for Mn_3CoSi at 295 K. Tick marks indicate the positions of Bragg reflections.

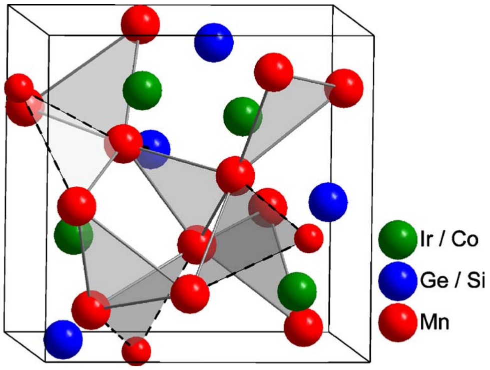

FIG. 3. (Color online) The crystal structure of $Mn_3Ir_{1-y}Co_ySi_{1-x}Ge_x$. Near neighbor Mn atoms form a network of corner sharing triangles (shaded). Three Mn atoms outside the unit cell (smaller, with hatched links) are added to complete the network.

tion patterns of Mn_3IrSi and Mn_3IrGe at 10 K. The observed intensities can be indexed by a magnetic unit cell of the same size as the crystallographic cell, and are well explained by the Mn_3IrSi type noncollinear antiferromagnetic structure with significant magnetic moments only on the Mn atoms. In the crystal structure, there is only one crystallographic site for Mn, the 12*b* site (general position) in the crystallographic space group $P2_13$. Similarly, all magnetic moments are symmetry related and can be generated from one magnetic moment vector by the symmetry operations of the magnetic space group $P2_13$ (No. 198.1.1511), using the survey of magnetic space groups compiled by Litvin, see Ref. 30. On the network of corner linked triangles formed by the near neighbor Mn atoms, the projections of the Mn magnetic moments on the triangle planes form 120° angles, see Fig. 6. The 120° angles are a result of geometric frustration of antiferromagnetic interactions, as previously discussed for Mn_3IrSi in Ref. 1, where a more detailed description of the magnetic structure was provided. For two of the three components of the magnetic moments along the crystallographic axes (M_x, M_y, M_z), the magnitudes differed less than three standard deviations and were therefore constrained to have equal magnitudes in the last cycles of refinements, resulting in decreased standard deviations for the magnetic moment components. The observed and calculated diffraction profiles for Mn_3CoGe at 10 K can be seen in Fig. 7 and the structural parameters and Mn magnetic moments obtained for Mn_3CoGe, $Mn_3CoSi_{0.50}Ge_{0.50}$, and $Mn_3Ir_{0.80}Co_{0.20}Si$ at 10 K are listed in Table IV. At 90 K the obtained Mn magnetic moments decreased to 2.05(3) and 1.59(2) μ_B for Mn_3CoGe and $Mn_3CoSi_{0.50}Ge_{0.50}$, respectively, with small variations of the atomic coordinates compared to those obtained at 10 K.

In the theoretical calculations of Mn_3CoGe (using the LMTO-ASA method) a magnetic moment of ~0.3 μ_B was found on Co, pointing along the [111] directions. If Co mo-

TABLE III. Interatomic distances (<3.2 Å) in $Mn_3Ir_{1-y}Co_ySi_{1-x}Ge_x$ at 295 K (from left to right in increasing unit cell volume order). Estimated standard deviations within parentheses.

	Distance (Å)				
Atoms	Mn_3CoSi	$Mn_3Ir_{0.20}Co_{0.80}Si$	$Mn_3CoSi_{0.50}Ge_{0.50}$	Mn_3CoGe	$Mn_3Ir_{0.80}Co_{0.20}Si$
Mn-2 Mn	2.571(9)	2.511(7)	2.645(7)	2.684(7)	2.68(1)
Mn-2 Mn	2.640(9)	2.644(7)	2.655(6)	2.685(8)	2.72(1)
Mn-2 Mn	2.665(9)	2.789(7)	2.673(6)	2.694(7)	2.72(1)
Mn-Ir/Co	2.53(1)	2.57(1)	2.559(9)	2.61(1)	2.653(7)
Mn-Ir/Co	2.60(1)	2.628(9)	2.630(9)	2.66(1)	2.701(7)
Mn-Ir/Co	2.680(5)	2.719(5)	2.708(4)	2.731(5)	2.731(6)
Mn-Si/Ge	2.568(9)	2.59(1)	2.610(4)	2.610(5)	2.62(1)
Mn-Si/Ge	2.607(9)	2.63(1)	2.635(5)	2.685(5)	2.69(1)
Mn-Si/Ge	2.622(5)	2.642(5)	2.659(4)	2.702(4)	2.766(6)
Ir/Co-3 Si/Ge	2.335(3)	2.350(3)	2.363(2)	2.392(2)	2.406(2)

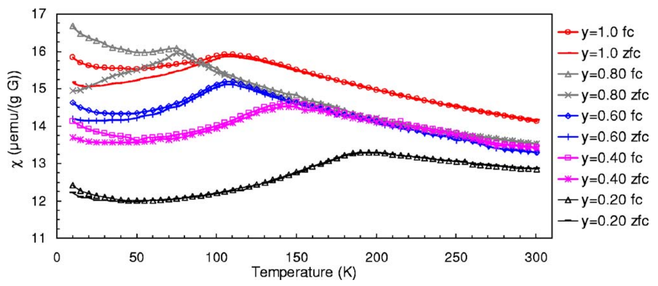

FIG. 4. (Color online) Temperature dependence of the field cooled (fc) and zero field cooled (zfc) magnetic susceptibility for $Mn_3Ir_{1-y}Co_ySi$: $y=1.0$, 0.80, 0.60, 0.40, and 0.20.

ments are included as variables in the magnetic structure refinements for Mn_3CoGe, the obtained Co moment magnitude is 0.4 μ_B (corresponding to three standard deviations), without significantly changing the Mn moment, and giving slightly lower agreement factors ($R_{wp}=4.85\%$, $R_{Bragg}=4.35\%$, $R_{Mag}=4.42\%$, compared to $R_{wp}=4.87\%$, $R_{Bragg}=4.40\%$, $R_{Mag}=4.89\%$ without a Co moment). Since the magnitude of the Co moment is too low to obtain accurate values from our refinements on neutron powder diffraction data, only the M_x, M_y, M_z magnetic moment components of the 12 Mn atoms within the unit cell are compared to the calculated values for Mn_3CoGe, see Table V (further discussed in the section describing the theoretical magnetic structure).

The neutron powder diffraction profiles recorded for Mn_3CoSi and $Mn_3Ir_{0.20}Co_{0.80}Si$ below the magnetic transition temperatures are markedly different from those obtained for the Mn_3IrSi type magnetically ordered samples. Figure 8(a) (lower panel) shows the diffraction profiles obtained for Mn_3CoSi at 295, 120, 75, and 10 K. The 295 K and 120 K patterns are very similar, whereas the 75 and 10 K patterns indicate onset of some type of magnetic order, as inferred from the presence of broad shoulders on the left-hand side of the (110) reflection and the right-hand side of the (210) reflection, with increased intensity at 10 K compared to 75 K. In addition a small increase of the background curvature can be noted under the Bragg peaks at $2\theta < 50°$ in the low temperature patterns. The temperature dependence is in agreement with the magnetic transition temperature of 100 K observed from magnetization measurements. It is interesting to note that the shoulders appear close to the two reflections with the largest magnetic contribution to the diffraction intensity for the Mn_3IrSi type noncollinear magnetic structure. The shoulders are fairly broad, so no well-defined magnetic long range order is expected. For $Mn_3Ir_{0.20}Co_{0.80}Si$, Fig. 8(b) (upper panel) shows a highly magnified section of the neutron powder diffraction profiles at 295 and 10 K, close to the base of the diffraction peaks. An increased curvature of the background can be noticed in the 10 K pattern compared to the 295 K pattern, most pronounced on the left-hand side of the (110) reflection, under the (111) reflection and on the right-hand side of the (210) reflection. This may be ascribed to onset of magnetic short-range order at low temperatures.

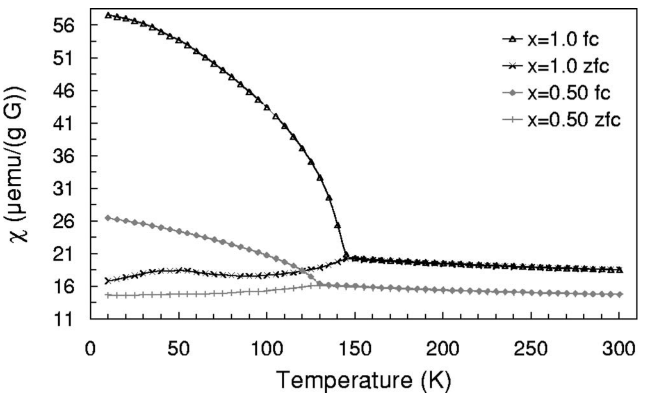

FIG. 5. Temperature dependence of the field cooled (fc) and zero field cooled (zfc) magnetic susceptibility for $Mn_3CoSi_{1-x}Ge_x$: $x=1.0$ and $x=0.50$.

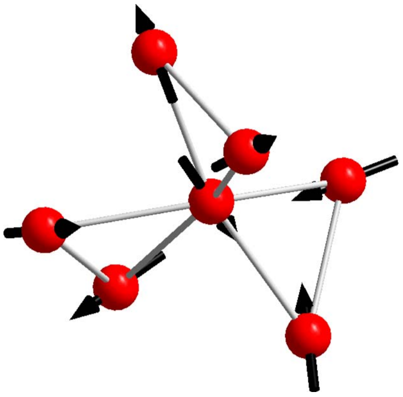

FIG. 6. (Color online) Orientation of the magnetic moments on three corner sharing triangles of Mn atoms.

E. Theoretical magnetic structure

Theoretical calculations were carried out for Mn_3CoSi and Mn_3CoGe. It should be noted that the experimental crys-

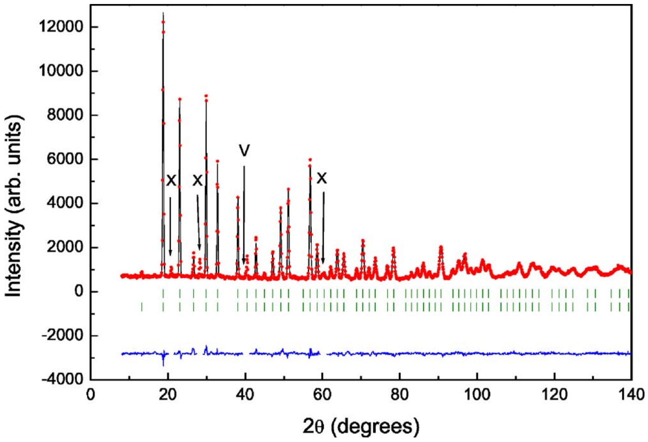

FIG. 7. (Color online) Observed (points), calculated (solid line) and difference (bottom solid line) neutron powder diffraction profiles for Mn_3CoGe at 10 K. Tick marks indicate the positions of Bragg reflections for the crystal structure (upper set) and the magnetic structure (lower set). The regions excluded from the refinement correspond to peaks from impurity phases (marked with "X"), and a minor peak from the vanadium sample holder, partly overlapping a peak from the crystal and magnetic structures (marked with "V").

TABLE IV. Structural parameters and magnetic moment for $Mn_3Ir_{1-y}Co_ySi_{1-x}Ge_x$ at 10 K. Estimated standard deviations within parentheses. Space group $P2_13$.

Atom	Wyckoff pos.	x	y	z	$M(\mu_B)$
			Mn_3CoGe		
Mn	12*b*	0.1254(6)	0.2022(5)	0.4532(7)	2.39(3)
Co	4*a*	0.6848(9)	0.6848	0.6848	
Ge	4*a*	0.0642(3)	0.0642	0.0642	
$B_{overall}$=0.16(2) Å^2 a=6.3742(2) Å					
R_p=3.67%; R_{wp}=4.87%; R_{exp}=3.21%; χ^2=2.31; R_{Bragg}=4.40%; R_{mag}=4.89%					
			$Mn_3CoSi_{0.50}Ge_{0.50}$		
Mn	12*b*	0.1245(6)	0.2012(5)	0.4534(6)	2.12(2)
Co	4*a*	0.6886(8)	0.6886	0.6886	
Si/Ge	4*a*	0.0655(3)	0.0655	0.0655	
$B_{overall}$=0.14(2) Å^2 a=6.3040(2) Å					
R_p=3.25%; R_{wp}=4.11%; R_{exp}=3.16%; χ^2=1.69; R_{Bragg}=4.58%; R_{mag}=4.66%					
			$Mn_3Ir_{0.80}Co_{0.20}Si$		
Mn	12*b*	0.1169(8)	0.203(1)	0.4564(8)	2.71(2)
Ir/Co	4*a*	0.6830(4)	0.6830	0.6830	
Si	4*a*	0.0638(9)	0.0638	0.0638	
$B_{overall}$=0.18(2) Å^2 a=6.4464(4) Å					
R_p=3.87%; R_{wp}=4.87%; R_{exp}=4.13%; χ^2=1.39; R_{Bragg}=5.37%; R_{mag}=3.37%					

tal structure parameters were used in these calculations. The calculation of Mn_3CoGe reproduces the experimentally observed noncollinear antiferromagnetic structure as regards the polar angles that determine the direction of each atomic projected magnetic moment and gives reasonable agreement of the size of the magnetic moments. The calculated values from the LMTO method are given in Table V and are here compared to experimental data and one may note that theory does not deviate from experiment with more than 15% concerning the magnitude of the moment and not more than a few degrees for the polar angles describing the magnetization directions. In calculations for Mn_3CoSi, using the LMTO method, the lowest energy was obtained for a noncollinear antiferromagnetic structure very similar to that of Mn_3CoGe, see Table VI for the calculated magnetic moments. However, with a slightly higher energy (~0.5 mRy/f.u.), a ferrimagnetic structure with a net moment of about 0.3 μ_B/f.u. was also found to be stable. Hence, the difficulty in identifying experimentally a magnetic structure for Mn_3CoSi may be connected to the possibility of several competing magnetic structures being nearly degenerate for this compound.

In order to analyze the mechanism that determines the magnetic noncollinear structure we show in Fig. 9 the electronic density of states (DOS) of Mn_3CoGe in a hypothetical ferromagnetic structure as well as in the experimentally observed noncollinear structure. This calculation used the noncollinear LMTO-ASA method. It may be noted that the DOS is dominated by the Mn contribution, which is natural since this element constitutes the largest atomic fraction of the compound. More importantly it may be seen that the noncollinear magnetic phase has fewer states in the vicinity of the Fermi level (E_F) and more states at lower energies. This may

TABLE V. Experimental and theoretical magnetic moments of Mn_3CoGe in x,y, and z components that describe the direction of the magnetic moment on each atom.

	Calculated			*Experiment*		
Atom[a]	M_x	M_y	M_z	M_x	M_y	M_z
Mn 1	1.21	1.77	−1.74	1.03(2)	1.52(2)	−1.52(2)
Mn 2	−1.21	−1.77	−1.74	−1.03(2)	−1.52(2)	−1.52(2)
Mn 3	−1.21	1.77	1.74	−1.03(2)	1.52(2)	1.52(2)
Mn 4	1.21	−1.77	1.74	1.03(2)	−1.52(2)	1.52(2)
Mn 5	−1.76	1.18	1.78	−1.52(2)	1.03(2)	1.52(2)
Mn 6	−1.76	−1.18	−1.78	−1.52(2)	−1.03(2)	−1.52(2)
Mn 7	1.76	−1.18	1.78	1.52(2)	−1.03(2)	1.52(2)
Mn 8	1.76	1.18	−1.78	1.52(2)	1.03(2)	−1.52(2)
Mn 9	1.75	−1.78	1.20	1.52(2)	−1.52(2)	1.03(2)
Mn 10	−1.75	−1.78	−1.20	−1.52(2)	−1.52(2)	−1.03(2)
Mn 11	1.75	1.78	−1.20	1.52(2)	1.52(2)	−1.03(2)
Mn 12	−1.75	1.78	1.20	−1.52(2)	1.52(2)	1.03(2)
Co 1	−0.19	−0.19	−0.19	[b]		
Co 2	0.19	0.19	−0.19			
Co 3	0.19	−0.19	0.19			
Co 4	−0.19	0.19	0.19			

[a] The Mn and Co atoms are numbered as the equivalent coordinates of the *12b* and *4a* site, respectively, in space group $P2_13$ in the International Tables for Crystallography.

[b] The Co moments are of too low magnitude to obtain accurate experimental values.

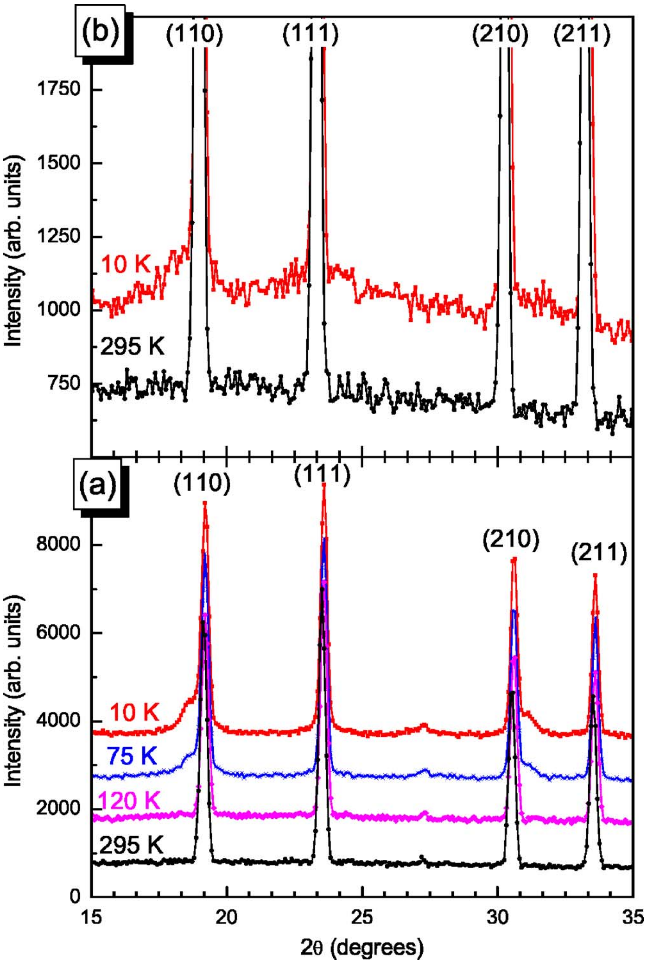

FIG. 8. (Color online) Neutron powder diffraction profiles for (a) Mn_3CoSi recorded at 295, 120, 75, 10 K, plotted with offset along the intensity axis. (b) $Mn_3Ir_{0.20}Co_{0.80}Si$ recorded at 295 and 10 K, with the 10 K data offset along the intensity axis (please note that only a fraction of the full peak intensity is shown, highly magnified, in order to more clearly illustrate the small differences in the background curvature).

TABLE VI. Theoretical magnetic structure model of Mn_3CoSi. The calculated total magnetic moments, and the x,y, and z components that describe the direction of the magnetic moment are listed.

Atom[a]	M_x	M_y	M_z	M_{tot}
Mn 1	1.01	1.50	−1.48	2.34
Mn 2	−1.01	−1.50	−1.48	2.34
Mn 3	−1.01	1.50	1.48	2.34
Mn 4	1.01	−1.50	1.48	2.34
Mn 5	−1.49	1.00	1.49	2.34
Mn 6	−1.49	−1.00	−1.49	2.34
Mn 7	1.49	−1.00	1.49	2.34
Mn 8	1.49	1.00	−1.49	2.34
Mn 9	1.48	−1.49	1.01	2.34
Mn 10	−1.48	−1.49	−1.01	2.34
Mn 11	1.49	1.49	−1.01	2.34
Mn 12	−1.48	1.49	1.01	2.34
Co 1	−0.10	−0.10	−0.10	0.18
Co 2	0.10	0.10	−0.10	0.18
Co 3	0.10	−0.10	0.10	0.18
Co 4	−0.10	0.10	0.10	0.18

[a] The Mn and Co atoms are numbered as the equivalent coordinates of the *12b* and *4a* site, respectively, in space group $P2_13$ in the International Tables for Crystallography.

simply be seen by inspecting the height of the DOS around E_F for the two magnetic configurations. The noncollinear magnetic phase has a rather large peak situated at lower energies, ~−0.2 Ry, a peak which is absent for the ferromagnetic configuration. Since the kinetic energy in DFT involves an integral $\int eD(e)de$, $[D(e)$=electronic density of states; e=energy$]$ it is clear that this contribution favors a configuration where the weight of the DOS is situated at low energies. This correlation is frequently encountered in the analysis of structural phase stability. Hence, the stability of the noncollinear magnetic phase can be associated to an electronic structure effect where in particular the kinetic energy contribution to the energy functional is important. It is important to point out that we have for simplicity only compared the ferromagnetic and experimental noncollinear magnetic structures, other configurations are of course also relevant to compare, e.g., an antiferromagnetic or ferrimagnetic collinear configuration. However, such an analysis tends to be lengthy and we have not pursued it. It should also be noted that the analysis we have pursued here relies on a DOS analysis, and is similar in nature to the analysis in Ref. 31, where a k space resolved quantity, i.e., the energy bands, was analyzed. In short, the argument in Ref. 31 (which in turn was based on Refs. 32 and 33) was that bands hybridize

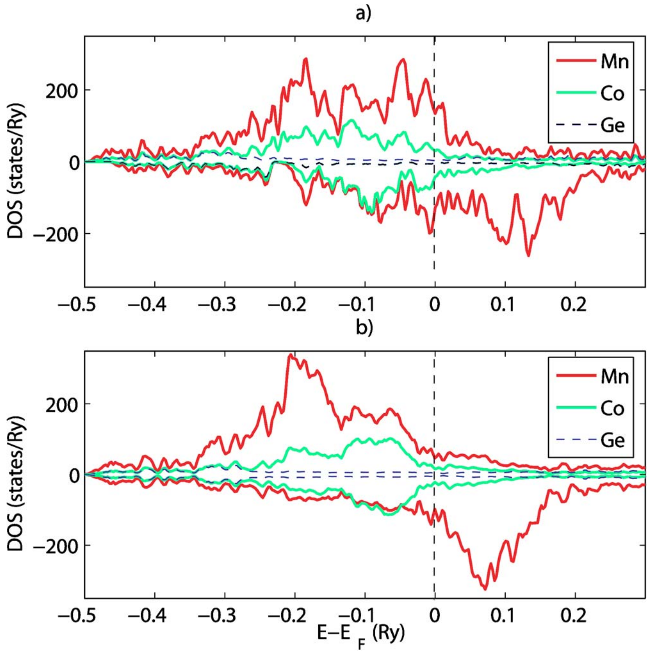

FIG. 9. (Color online) The calculated density of states (DOS) of Mn_3CoGe in (a) ferromagnetic configuration, (b) noncollinear configuration. The energies are given relative to the Fermi level, which is indicated by a dashed line.

for the noncollinear magnetic order, opening up band gaps around E_F, so that the number of bands that cross E_F is reduced, the total energy of the system is lowered, and the noncollinear configuration is stabilized over the collinear magnetic structure. The reason for why we performed a k-space integrated analysis here (i.e., the DOS) is purely practical, since the presently studied compounds generate a very high amount of energy bands which become difficult to analyze graphically. In addition it should be remarked that nearest neighbor antiferromagnetic exchange interactions on a frustrated lattice often lead to a noncollinear magnetic order.[33]

V. DISCUSSION AND CONCLUSIONS

Two new ternary compounds, Mn_3CoSi and Mn_3CoGe, are found to be isostructural with the previously reported Mn_3IrSi and Mn_3IrGe ($AlAu_4$ type structure; an ordered form of the β-Mn structure). In a similar fashion to the situation between Mn_3IrSi and Mn_3IrGe, a complete range of solid solubility is demonstrated between Mn_3CoSi and Mn_3CoGe as well as between Mn_3CoSi and Mn_3IrSi.

Mn_3IrGe, Mn_3IrSi, $Mn_3Ir_{0.80}Co_{0.20}Si$, Mn_3CoGe, and $Mn_3CoSi_{0.50}Ge_{0.50}$ are found to order magnetically in the same noncollinear antiferromagnetic structure, with a magnetic unit cell equal to the crystallographic cell. The Mn atoms form a three-dimensional network of corner linked triangles, on which the projections of the magnetic moments are rotated 120° around the triangle axes. In contrast, this magnetic structure is not found for the two compounds of smallest unit cell volumes, namely $Mn_3Ir_{0.20}Co_{0.80}Si$ and Mn_3CoSi. For $Mn_3Ir_{0.20}Co_{0.80}Si$ diffuse scattering features appearing at low temperatures suggest short-range magnetic correlations, whereas for Mn_3CoSi the diffraction patterns recorded below the magnetic transition temperature display more distinct (albeit still relatively broad) shoulders on the nuclear diffraction peaks. This may suggest that a transformation to a new type of magnetic structure, incommensurate with the crystallographic unit cell, has started on decreasing the unit cell volume below that of $Mn_3CoSi_{0.50}Ge_{0.50}$, although completely well defined long-range order is not achieved. This observation is not inconsistent with the theoretical finding of a (or possibly several) ferrimagnetic structure that for Mn_3CoSi competes with the 120° spin structure.

In view of the reported lack of magnetic order in β-Mn, as further discussed below, it is interesting to note that the unit cell parameter of β-Mn (values in the range $a=6.29$–6.315 Å are found in the literature[27,34–36]) is very similar to the unit cell parameters of both the magnetically ordered compound $Mn_3CoSi_{0.50}Ge_{0.50}$ [$a=6.3219(2)$ Å at 295 K], and the (possibly) short-range magnetically ordered $Mn_3Ir_{0.20}Co_{0.80}Si$ [$a=6.2992(2)$ Å at 295 K].

As was illustrated by Fig. 4, the magnetic transition temperature of the samples varies with composition. An alternative illustration of this variation is given in Fig. 10, where the transition temperature of three different sample series ($Mn_3IrSi_{1-x}Ge_x$, $Mn_3Ir_{1-y}Co_ySi$, and $Mn_3CoSi_{1-x}Ge_x$) is plotted vs lattice parameter. The magnetic properties of $Mn_3IrSi_{1-x}Ge_x$ have been reported before,[1,2] and are included here for reference only. Also plotted in the figure is the calculated interatomic exchange energy J_0 for four of these samples (Mn_3IrGe, Mn_3IrSi, Mn_3CoGe, and Mn_3CoSi). We note in passing that the KKR-ASA method was used for this calculation. Disregarding details of the behavior, there is a good correspondence, both as regards trend and magnitude, between the decrease of the transition temperatures and the decay of the exchange energy.

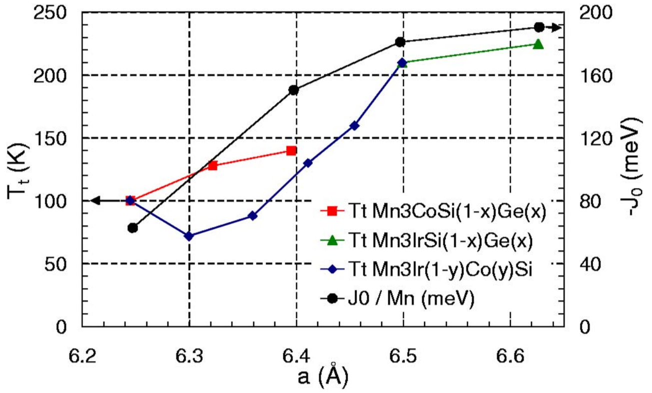

FIG. 10. (Color online) Experimental magnetic transition temperature (T_t), in K, and the calculated exchange energy per Mn atom (J_0), in meV, plotted as a function of the lattice parameter, in Å.

The magnitude of the magnetic moment on Mn shows a closely linear dependence on the unit cell parameter. This is shown in Fig. 11 where we compile our experimental and theoretical findings (with the previously reported[1,2] magnetic properties of Mn_3IrSi and Mn_3IrGe included for reference). Note that the theoretical values in the figure are obtained at the experimental volume, except for Mn_3IrSi, where for comparison we calculated the magnetic moments also for the volumes of Mn_3IrGe, Mn_3CoSi, and Mn_3CoGe. The volumes of these compounds are such that Mn_3IrGe has the largest lattice parameter, then comes Mn_3IrSi, then Mn_3CoGe, whereas Mn_3CoSi is smallest. The magnetic moment is larger for the largest volumes, since a material at larger vol-

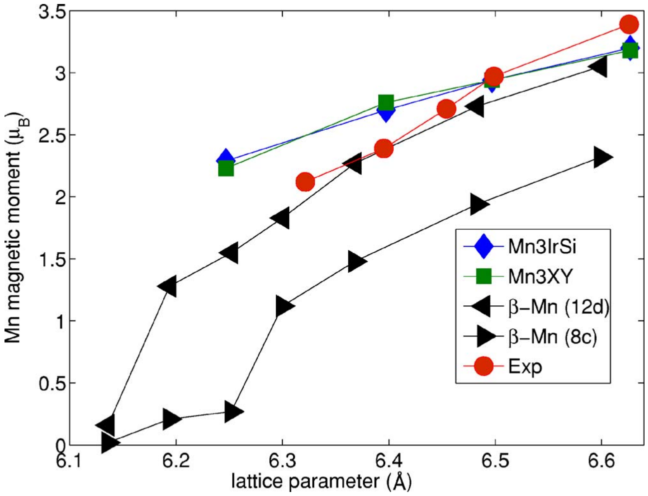

FIG. 11. (Color online) Mn magnetic moments, in μ_B/atom, as a function of the lattice parameter, in Å.

umes have smaller overlap between atomic centered wave functions, and hence narrower energy bands, which always results in larger magnetic moments.[33] It is interesting to note that both experiment and theory follow each other closely in Fig. 11, although the experimental curve drops off somewhat faster with reduced volume compared to the calculated curve. It is also interesting to note that the calculated moments of Mn_3IrSi agree very closely with any other compound in our studied series, provided the volumes are equal. This indicates that the magnetic properties of these systems are heavily influenced by the interatomic distance.

The calculated trend of the magnetism of β-Mn is very similar to that of Mn_3IrGe, Mn_3IrSi, Mn_3CoGe, and Mn_3CoSi, especially the large magnetic moments on the Mn atoms at the β-Mn $12d$ site, which for both β-Mn and the Mn_3XY compounds (X=Ir, Co; Y=Si, Ge) form an identical three-dimensional network of triangles. The moments at the β-Mn $8c$ site are found to be much smaller, and since it is this site the Si, Ge, Ir, and Co atoms occupy, we can not make a comparison to the magnetic moments in Mn_3IrSi, Mn_3IrGe, Mn_3CoSi, and Mn_3CoGe. However, it is interesting to note that replacing a magnetic element (Mn at the $8c$ site) with nonmagnetic elements, causes the appearance of magnetic order, contrary to expectations. Further, since the same three-dimensional network of Mn triangles is formed by the β-Mn $12d$ site as the Mn atoms of the Mn_3XY compounds, our observations of long-range magnetic order on this triangular network in the Mn_3XY compounds suggest that for β-Mn geometric frustration on the network of triangles should not alone be responsible for its lack of magnetic order, contrary to previous analyses by, e.g., Shiga *et al.*[37] and Nakamura *et al.*[4] It should also be noted here that, in agreement with the calculation of Hafner and Hobbs,[13] we find a ferrimagnetic configuration to be stabilized in β-Mn, for all volumes. Hence the magnetic Mn atoms at the $8c$ site contribute with an exchange field also on the Mn atoms at the $12d$ site and one may speculate that this disrupts the antiferromagnetic interaction among the Mn atoms of the $12d$ site, such that the strong noncollinear magnetic structure observed, e.g., for Mn_3CoGe is replaced with something else. The details of this are at the moment not known exactly, but we note that our analysis of the magnetic interactions in the presently studied intermetallic compounds and β-Mn are not inconsistent with the spin liquid analysis of Refs. 4 and 5.

We end with an analysis that leads to the prediction of a pressure induced magnetic transition from a paramagnetic state of β-Mn to a magnetically ordered state. According to Fig. 11, on decreasing unit cell parameter the Mn moment of the $8c$ site decreases to a negligible magnitude much faster than the Mn moment of the $12d$ site. For instance, at a lattice constant of 6.25 Å the Mn moment of the $8c$ site is less than 0.25 μ_B/atom whereas the Mn moment at the $12d$ site is $\sim$1.5 μ_B/atom. Hence at this volume there is a great similarity between β-Mn and, e.g., Mn_3CoGe in the sense that the exchange field from the atoms at the $8c$ site is absent (or small), and we expect a dominating antiferromagnetic interaction among the Mn atoms at the $12d$ site. With magnetic interactions only on the three-dimensional network of triangles formed by the $12d$ site atoms, one may expect formation of magnetic order in β-Mn, similar to, e.g., Mn_3CoGe or Mn_3CoSi. Hence one could envision that as a function of pressure, with a 3% decrease of the unit cell volume, β-Mn could undergo a transition to a magnetically ordered state from a nonordered state, something which is contrary to all previous experience. Such studies are underway.

ACKNOWLEDGMENTS

Håkan Rundlöf is acknowledged for skillful assistance in neutron powder diffraction data collection. Parts of the calculations were performed at the High Performance Computer Center North (HPC2N) in Umeå, Sweden. Financial support from the Swedish Research Council (VR) and the Swedish Foundation for Strategic Research (SSF) is acknowledged.

---

[1] T. Eriksson, R. Lizárraga, S. Felton, L. Bergqvist, Y. Andersson, P. Nordblad, and O. Eriksson, Phys. Rev. B **69**, 054422 (2004).

[2] T. Eriksson, L. Bergqvist, P. Nordblad, O. Eriksson, and Y. Andersson, J. Solid State Chem. **177**, 4058 (2004).

[3] J. S. Kasper and B. W. Roberts, Phys. Rev. **101**, 537 (1956).

[4] H. Nakamura, K. Yoshimoto, M. Shiga, M. Nishi, and K. Kakurai, J. Phys.: Condens. Matter **9**, 4701 (1997).

[5] J. R. Stewart and R. Cywinski, Phys. Rev. B **59**, 4305 (1999).

[6] J. R. Stewart and R. Cywinski, J. Magn. Magn. Mater. **272-276**, 676 (2004).

[7] J. B. Dunlop, J. M. Williams, and J. Crangle, Physica B & C **86–88**, 269 (1977).

[8] Y. Nakai, J. Phys. Soc. Jpn. **63**, 775 (1994).

[9] T. Hori, J. Phys. Soc. Jpn. **38**, 1780 (1975).

[10] S. Funahashi and T. Kohara, J. Appl. Phys. **55**, 2048 (1984).

[11] K. Sasao, R. Y. Umetsu, and K. Fukamichi, J. Alloys Compd. **325**, 24 (2001).

[12] M. Miyakawa, R. Y. Umetsu, K. Sasao, and K. Fukamichi, J. Phys.: Condens. Matter **15**, 4605 (2003).

[13] J. Hafner and D. Hobbs, Phys. Rev. B **68**, 014408 (2003).

[14] Y. B. Kuz'ma, Russ. J. Inorg. Chem. **7**, 691 (1962).

[15] Y. B. Kuz'ma and E. I. Gladyshevskii, Russ. J. Inorg. Chem. **9**, 373 (1964).

[16] D. I. Bardos, R. K. Malik, F. X. Spiegel, and P. A. Beck, Trans. Metall. Soc. AIME **236**, 40 (1966).

[17] The computer code was made in-house, based on the original method published in O. K. Andersen, Phys. Rev. B **12**, 3060 (1975); and H. L. Skriver, *The LMTO method* (Springer, Berlin, 1984).

[18] S. Rundqvist, Chem. Scr. **28**, 15 (1988).

[19] J. Rodríguez-Carvajal, FULLPROF computer program, version 2.80, LLB, Saclay (2004).

[20] P. J. Brown, in *International Tables for Crystallography*, Vol. C, edited by A. J. C. Wilson (The International Union of Crystallography, London, 1992).

[21] I. A. Abrikosov and H. L. Skriver, Phys. Rev. B **47**, 16532 (1993).

[22] A. V. Ruban and H. L. Skriver, Comput. Mater. Sci. **15**, 119 (1999).

[23] M. Methfessel and A. T. Paxton, Phys. Rev. B **40**, 3616 (1989).

[24] J. P. Perdew, K. Burke, and M. Ernzerhof, Phys. Rev. Lett. **77**, 3865 (1996).

[25] A. I. Liechtenstein, M. I. Katsnelson, V. P. Antropov, and V. A. Gubanov, J. Magn. Magn. Mater. **67**, 65 (1987).

[26] O. E. Ullner, Ark. Kemi, Mineral. Geol. **14A**, 1 (1940).

[27] G. D. Preston, Philos. Mag. **5**, 1207 (1928).

[28] J. Mattsson, C. Djurberg, and P. Nordblad, J. Magn. Magn. Mater. **136**, L23 (1994).

[29] M. Lederman, J. Hammann, and R. Orbach, Physica B **165-166**, 179 (1990).

[30] D. B. Litvin, Acta Crystallogr., Sect. A: Found. Crystallogr. **A57**, 729 (2001). The complete tables entitled Magnetic Space Group Types is available from the IUCr electronic archives, reference DR0012.

[31] T. Eriksson, L. Bergqvist, T. Burkert, S. Felton, R. Tellgren, P. Nordblad, O. Eriksson, and Y. Andersson, Phys. Rev. B **71**, 174420 (2005).

[32] R. Lizárraga, L. Nordström, L. Bergqvist, A. Bergman, E. Sjöstedt, P. Mohn, and O. Eriksson, Phys. Rev. Lett. **93**, 107205 (2004).

[33] J. Kübler, *Theory of Itinerant Electron Magnetism* (Oxford Science Publications, Oxford, 2000).

[34] A. Westgren and G. Phragmén, Z. Phys. **33**, 777 (1925).

[35] S. J. Carlile, J. W. Christian, and W. Hume-Rothery, J. Inst. Met. **76**, 169 (1949).

[36] C. B. Shoemaker, D. P. Shoemaker, T. E. Hopkins, and S. Yindepit, Acta Crystallogr., Sect. B: Struct. Crystallogr. Cryst. Chem. **B34**, 3573 (1978).

[37] M. Shiga, K. Yoshimoto, H. Nakamura, and H. Wada, Int. J. Mod. Phys. B **7**, 1008 (1993).